*M. W. Brown**

Interfaces Between Short, Long, and Non-Propagating Cracks

REFERENCE Brown, M. W., **Interfaces Between Short, Long, and Non-Propagating Cracks**, *The Behaviour of Short Fatigue Cracks*, EGF Pub. 1 (Edited by K. J. Miller and E. R. de los Rios) 1986, Mechanical Engineering Publications, London, pp. **423–439**.

ABSTRACT A wide range of experimental techniques is used to study fatigue crack behaviour, covering the regimes of (a) long cracks (LEFM), (b) high strain fatigue, (c) microstructurally short cracks, and (d) non-propagating cracks. A full range of stress levels and crack lengths have been considered to show where each mechanism for crack extension is valid, what modes of crack tip opening operate, and what model is appropriate for describing crack growth rate. A fatigue diagram is developed to illustrate six regimes of fatigue crack behaviour, and this is contrasted with the Kitagawa–Takahashi diagram for finite/infinite life fatigue.

Notation

A	Constant, A > 2, for Mode I/III transition
a	Crack length
d	Spacing between microstructural barriers
E	Young's modulus
K	Stress intensity factor
k	Cyclic strength coefficient
N	Number of cycles
n	Cyclic strain hardening exponent
x	Percentage deviation of strain from LEFM formulation
Y	Geometry factor
Δ	Range of stress or strain
ε	Strain
σ	Stress

Subscripts

fl	Fatigue limit
M	Microstructural/continuum transition
PSB	Threshold stress for PSB nucleation
th	Threshold
u	Ultimate strength
y	Yield or proof stress

Introduction

The failure of metals by fatigue has received extensive industrial attention and academic research activity for many years, with a variety of methods being

* Department of Mechanical Engineering, University of Sheffield, Mappin Street, Sheffield, UK.

developed to observe the behaviour of fatigue cracks. Different disciplines from mathematics to metallurgy have come together to tackle this problem, each bringing their own areas of insight, but the unification of results from different laboratories has been largely overlooked, due primarily to the vast amount of literature published. However the overriding importance of the mechanisms of cyclic crack extension to the deterioration of metals in fatigue has been firmly established; therefore this paper attempts firstly to list the different types of propagation experimentally observed, and secondly to quantify the regimes within which each mechanism is dominant. Such mechanisms are rarely contrasted because they are usually studied in different types of laboratory test, namely those concerned with (a) high strain fatigue, (b) linear elastic fracture mechanics, (c) the behaviour of notches, (d) threshold experiments, and (e) fractographic analyses employing the surface replication technique.

All but one of these areas of investigation fall under the heading of 'short' cracks, even though the crack lengths involved differ by orders of magnitude. The exception is the linear elastic fracture mechanics (LEFM) case, for which propagating cracks at low levels of stress are termed 'long' cracks. Notwithstanding the normal usage of the word 'short', a long crack can become short simply by raising the level of applied stress in order to violate the allowable limits of LEFM. So in this instance the term 'short' has no relationship to the actual size of the crack, but rather it describes the intensity of load or degree of plasticity experienced.

This paper is limited to cracks growing in plain specimens. However the concepts may be extended to cover notched specimens if the effect of the stress gradient due to the notch can be taken into account. The behaviour of microstructurally short cracks, high strain or elasto-plastic fracture mechanics cracks, and non-propagating cracks are discussed briefly, but more detailed reviews have been published elsewhere (**1**)–(**4**).

The Kitagawa–Takahashi diagram

A significant advance in the understanding of short crack behaviour was made by Kitagawa and Takahashi (**5**), who proposed a diagram to show the effect of defect size on the fatigue limit stress, see, for example, Fig. 1. For large defects, the allowable stress for infinite life must be low, within the linear elastic fracture mechanics regime, and, therefore, the limiting condition is given by a straight line of slope minus one half corresponding to the threshold stress intensity factor ΔK_{th}, such that

$$\Delta K_{th} = Y \cdot \Delta\sigma\sqrt{(\pi a)} \qquad (1)$$

At the other end of the spectrum, for vanishingly small defects the allowable stress level must relate to the plain specimen fatigue limit. The Kitagawa–Takahashi diagram for the medium carbon steel in Fig. 1 shows the observed behaviour between these two extremes.

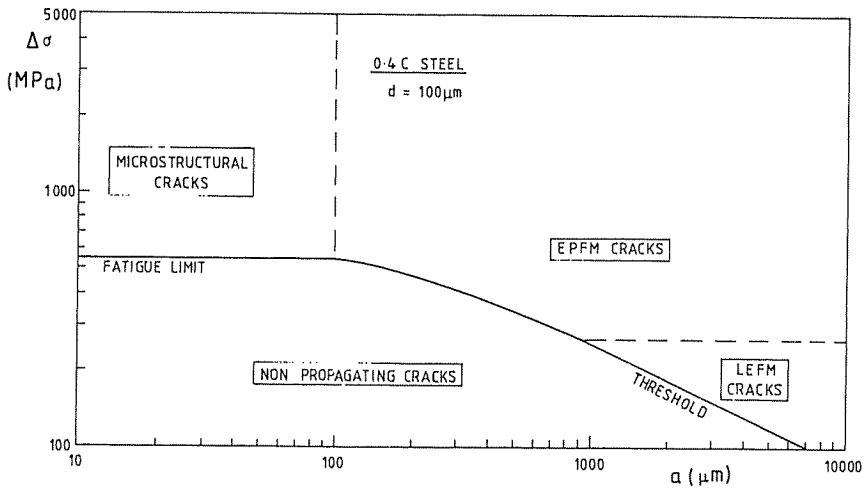

Fig 1 A Kitagawa–Takahashi diagram

Deviation from the LEFM straight line can usually be observed for peak stress levels above one third of the yield stress. Throughout this paper, we will be concerned with fully reversed cycling only, or zero mean stress. Thus the limiting stress range, $\Delta\sigma$, for LEFM behaviour will be two thirds of the yield stress. This requirement arises from the necessity for small scale yielding only at the crack tip if the LEFM characterization of crack tip stress conditions is to be valid. The basis of the description of fatigue crack propagation by the stress intensity factor range, ΔK, is that crack extension is governed by an elastic stress field at the crack tip, which determines various parameters such as plastic zone size and crack opening displacement. For small scale yielding, the plastic zone size is generally taken to be less than one fiftieth of the crack length (**6**). Note that this corresponds to a 1.5 per cent error in the elastic stress field for a centre-cracked panel, and as much as 7 per cent for a compact tension specimen. Since the plane strain plastic zone size is approximately one third of the plane stress value (**6**), one may write, for LEFM validity

$$(K_I/\sigma_y)^2/6\pi \leqslant 0.02a \qquad (2)$$

But for a crack with a geometry factor, Y, equal to unity

$$K_I = \sigma\sqrt{(\pi a)}$$

which, on substitution into equation (2), gives approximately

$$\sigma/\sigma_y \leqslant 1/3 \qquad (3)$$

Once this stress limit is exceeded, the errors in stress values derived from the stress intensity factor will build up rapidly, and therefore one should strictly use

elasto-plastic fracture mechanics (EPFM), for which a variety of parameters have been proposed to correlate fatigue crack growth behaviour (**2**). Even in the EPFM regime, a threshold condition can be observed (**5**), below which cracks are unable to grow, giving rise to the non-propagating crack regime in Fig. 1.

A fourth regime for crack growth can be identified in Fig. 1, where the cracks are sufficiently small to interact markedly with the microstructure. This strong dependence on microstructure may be associated with the fatigue limit (**7**), and the insensitivity of fatigue strength to small defect sizes shown by the Kitagawa–Takahashi diagram can be related to the ease of fatigue crack growth in the first grain where the crack initiates (**8**). Thus the use of the continuum based discipline of fracture mechanics is inappropriate for this regime.

Continuum and microstructural crack growth

The behaviour of propagating short cracks is typically presented in the literature using graphs of crack length versus crack growth rate, as shown in Fig. 2. An initial period of decelerating crack growth is frequently observed (**1**), where the minimum growth rate corresponds to the crack tip meeting some barrier to growth. However, if the crack has sufficient driving force to pass through that barrier, then a period of accelerating growth ensues until fracture takes place. The most common representation of this behaviour employs logarithmic axes (**1**)(**7**)(**9**)(**10**), as in Fig. 2(a), since this choice for the abscissa facilitates comparison of the accelerating, or EPFM, phase with the LEFM parameter, ΔK. However, a better understanding of the nature of microstructural crack growth (MCG) is gained from Fig. 2(b), which uses linear scales.

Figure 2 has been constructed from the equations for EPFM and MCG cracks derived empirically by Hobson (**11**)(**12**). Working on a medium carbon steel with uniaxial low cycle fatigue specimens, Hobson was able to derive the short crack growth characteristics from surface replication studies, which provided a detailed history of each crack. The MCG phase was described by the equation

$$da/dN = 153620(\Delta\varepsilon)^{3.51}(d - a) \tag{4}$$

where d, a and da/dN each have the same units for length. Here a is the surface crack length determined by replication, and d, the distance between the microstructural barriers for each end of the individual crack monitored, is found by fitting equation (4) to the data. Details of the material, test procedures, the relationship between d and the microstructure, and derivation of equation (4) are given elsewhere (**11**)(**12**).

For cracks spanning a number of grains, the effect of individual barriers to growth is small (**13**), and a continuum mechanics representation may be employed. Hobson derived the simple equation

$$da/dN = 4.102(\Delta\varepsilon)^{2.06}a - 4.237 \tag{5}$$

where da/dN is in nm/cycle, and a is in nm. This equation describes both LEFM

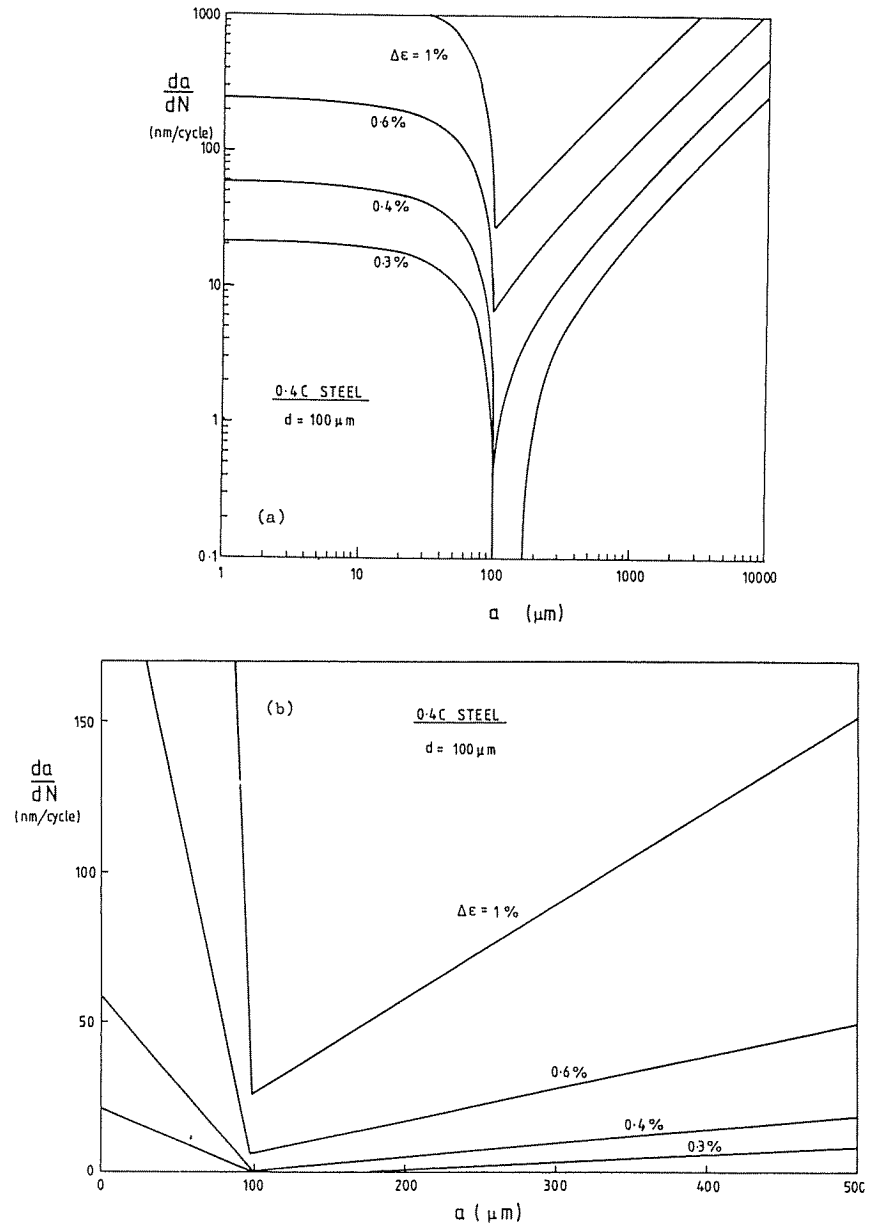

Fig 2 Growth of short cracks on (a) logarithmic axes, and (b) linear axes

behaviour and EPFM crack advance by adopting a form widely used in EPFM studies (**2**), but with the addition of a small threshold term.

Equations (4) and (5) have been used to construct Fig. 2, taking a nominal value for d in a medium carbon steel of 100 μm. This compares favourably with values measured by Hobson (**11**). The growth rate was chosen as the greatest of those determined from equations (4) and (5), respectively, for any given value of strain range, following the crack propagation criterion of Pineau *et al.* (**14**) that a crack will always adopt the mechanism that gives the fastest growth rate (**15**). The change in mechanism on reaching 100 μm crack length should correspond to the transition from Stage I to Stage II growth, depicted in Fig. 3 (**15**).

Stage I or MCG is typically a shear mode of cracking strongly associated with crystallographic planes. If a Stage I crack traverses two grains, a slight change of plane will be noticed at the first grain boundary. Similarly, MCG can cover two grains where a low angle boundary is involved, since a low angle boundary fails to provide a significant barrier to propagation (**13**)(**16**). Thus equation (4) appears to relate to the Stage I crack growth process.

However, Stage II cracking, or striation crack growth, is well known as a Mode I controlled mechanism, with a fracture surface normal to the maximum principal stress (**15**)(**17**). This clearly relates to a different plane to the MCG phase, so that a sharp transition in growth rate also, as predicted in Fig. 2, can be expected to occur in practice. Note that the early portion of Stage II propagation may have, faceted appearance indicating a crystallographic dependence, before the clear striation mechanism is able to operate (**18**). Nevertheless, this slow Mode I growth in the near threshold regime is normally described

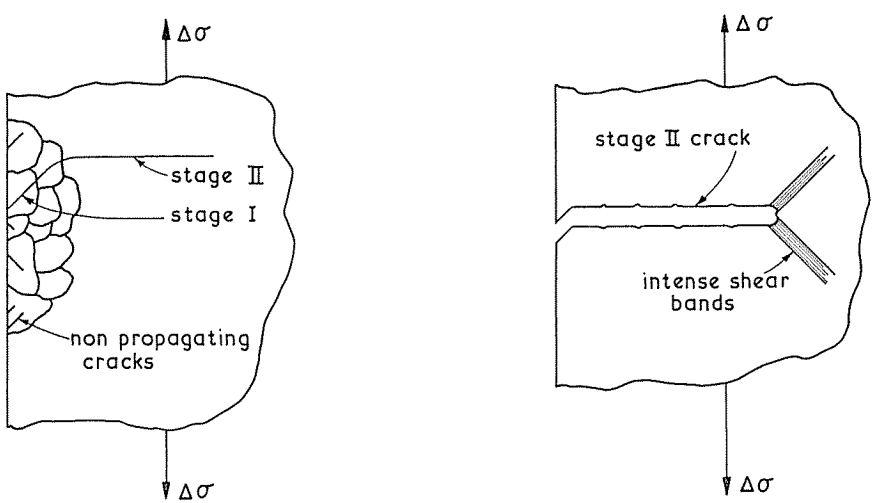

Fig 3 Two stages of fatigue crack growth

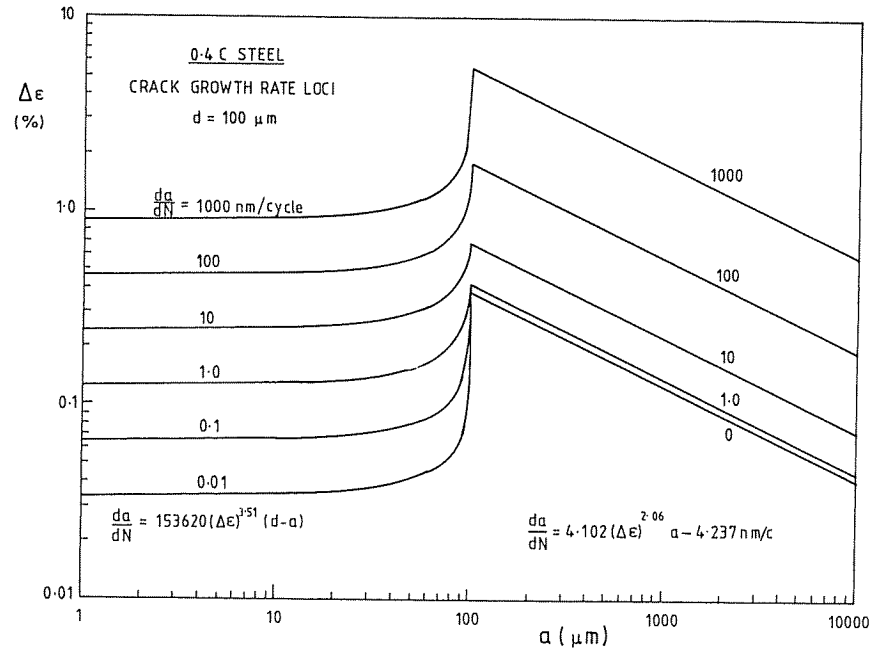

Fig 4 Crack propagation rates for strain controlled fatigue

by a fracture mechanics formulation. Thus equation (5) relates to the EPFM or Stage II growth regime.

Having derived the two crack growth equations above, an alternative method of presenting crack growth rate loci may be developed, as in Fig. 4. For any strain range applied to a crack of length a, the relevant mechanism for fatigue may be derived from Pineau's criterion, see above, and the growth rate determined. Contours or loci of constant growth rate have been plotted in Fig. 4, to show a clear demarcation between the two regimes of short crack growth, namely those of MCG and EPFM.

The fatigue diagram in Fig. 4 may be used to predict the history of a crack in a constant amplitude low cycle fatigue test. For example, for a strain range of 0.6 per cent, a crack growth rate of about 250 nm/cycle will be observed at the start of a test for a specimen with small initial defects (<1 μm). This growth rate will be essentially constant up to 20 μm crack length, as can be seen by sketching a horizontal line on Fig. 4 at $\Delta\varepsilon = 0.6$ per cent, since the loci plotted are essentially flat and parallel to this line. Thus in only 80 cycles, the crack will attain 20 μm length, followed by a period of deceleration to just 2.5 per cent of its initial speed. However, the change in mechanism to Mode I growth enables the crack to accelerate, and it will continue to accelerate up to failure. Figure 5 depicts the crack history for various strain ranges.

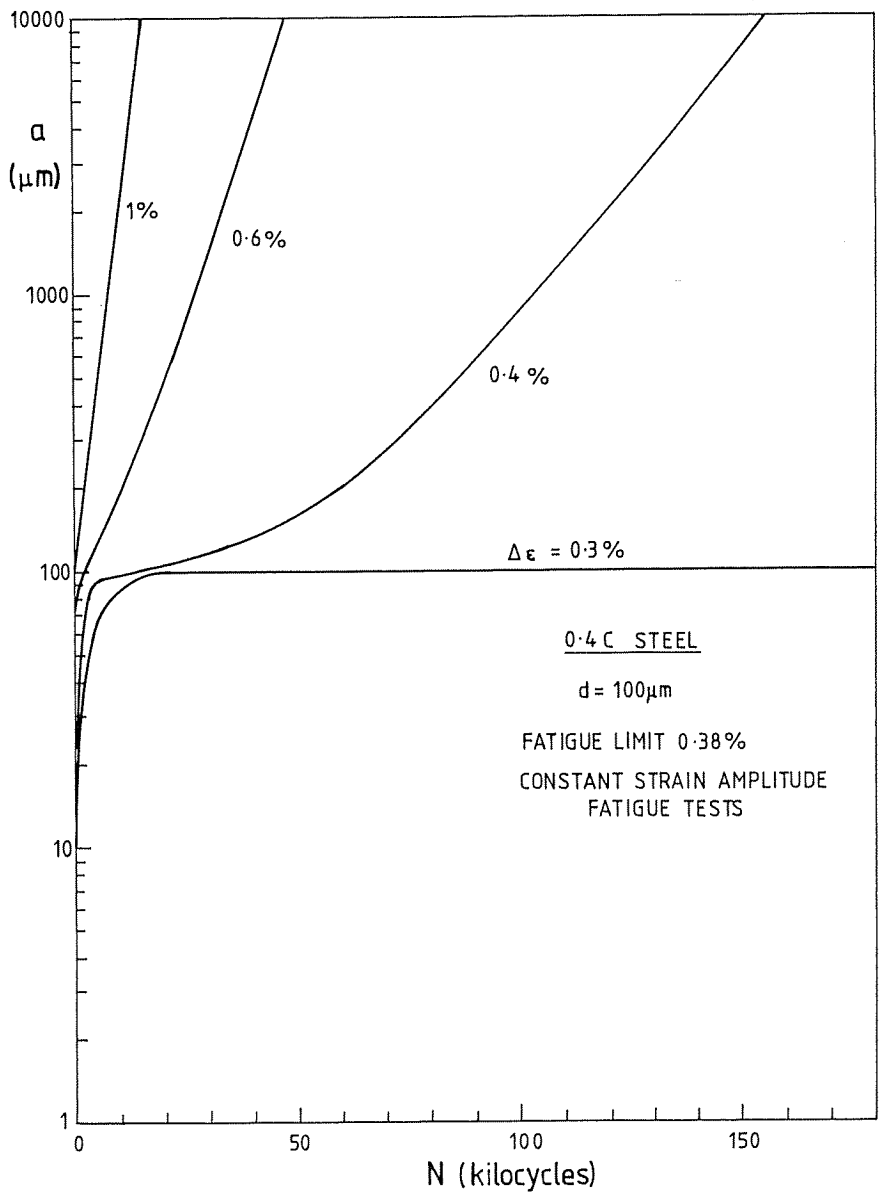

Fig 5 Predicted crack histories for constant amplitude fatigue tests

The case of $\Delta\varepsilon = 0.3$ per cent is of interest since it falls below the fatigue limit, and no transition to EPFM growth can be obtained (**19**). Such a specimen will contain non-propagating cracks of length 99 μm after only 21 500 cycles. The fatigue limit condition is clearly governed by the threshold value, together with critical crack length, d, of 100 μm. From equation (5), for zero crack growth rate, putting a equal to d

$$0 = 4.102(\Delta\varepsilon)^{2.06} \times 10^5 - 4.237 \tag{6}$$

which gives 0.38 per cent for the fatigue limit strain range (550 MPa stress range).

The fatigue diagram in Fig. 4 could also be used to derive variable strain amplitude crack histories, or even to deal with stress gradients due to notches or thermal stresses. Here the horizontal line used for the constant strain amplitude case should be replaced by a curve to depict the actual load history, or the stress gradient in a component. Such an approach, although a simplification of real behaviour, has been applied to EPFM cracks under cyclic thermal stress (**20**).

The fatigue and Kitagawa–Takahashi diagrams

Figure 4, a graph of strain range versus crack length, has a clear affinity to the Kitagawa–Takahashi diagram in terms of stress range. In order to provide a direct comparison, the cyclic stress–strain curve was used to replot Fig. 4 in terms of stress, as shown in Fig. 6.

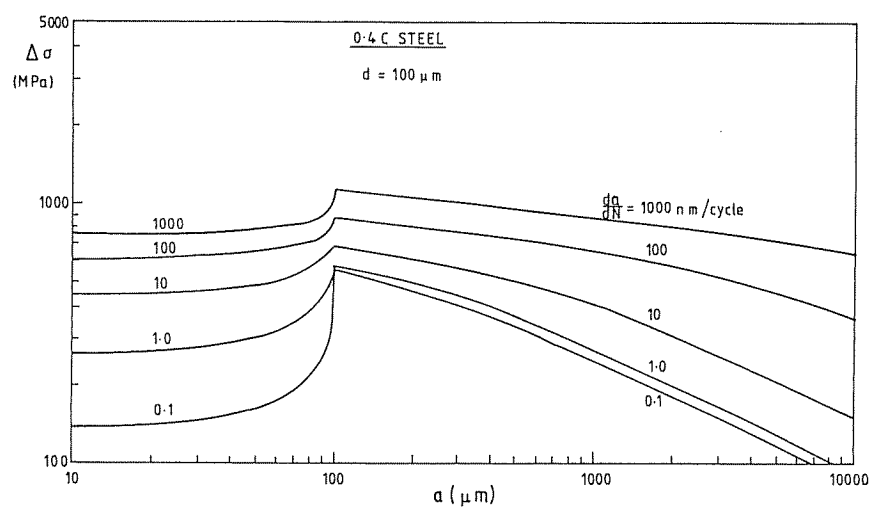

Fig 6 Crack propagation rates for stress controlled fatigue

It was assumed that the Ramberg–Osgood formulation of cyclic behaviour was applicable (**11**), such that

$$\Delta\varepsilon = \Delta\sigma/203\,000 + (\Delta\sigma/2013)^{1/0.190} \quad (7)$$

where the stress is given in MPa, and 0.19 is the strain hardening coefficient. Equation (7) gave reasonable fit to the stable half-life stress range measured in strain controlled experiments, and also to a multiple step test (**12**).

Comparison of Figs 1 and 6 shows that the Kitagawa–Takahashi line between non-propagating and fracture mechanics cracks corresponds closely with the 0.1 nm/cycle contour, i.e., the threshold condition. (Note 0.1 nm/cycle is widely used as a practical definition in the determination of threshold values.) Indeed the contours for 0 and 0.1 nm/cycle were so close that they could not be shown separately with the scales used in Fig. 6.

The fatigue limit from equation (6) gives a stress range of 550 MPa, as plotted in Fig. 1. This compares favourably with an experimentally measured value of 487 ± 15 MPa for a very similar batch of 0.4C steel (**21**). However, the discrepancy between these values is due to the arbitrary choice of d as 100 μm in Fig. 6, so that this figure represents the behaviour of a particular crack that initiates in a given grain where d = 100 μm. Clearly a representative value for d must be derived if the actual fatigue limit of a material is to be obtained. Now Hobson (**12**) found a mean value of d from 35 measurements, being 116 μm with a standard deviation of 51 μm. Thus a reasonably large well-orientated grain in a polycrystalline metal would probably correspond to a value for d of the mean plus one standard deviation, i.e., 167 μm, and a grain of about this size should initiate the failure crack that governs the material fatigue limit. A value of 167 μm for d predicts a fatigue strength, $\Delta\sigma$, of 486 MPa from equations (6) and (7).

Note that the deviation from linearity in Fig. 6 for the EPFM lines on leaving the LEFM regime derives purely from the cyclic stress–strain curve, if the formulation of the crack growth law in equation (5) is taken to be accurate. If the cyclic yield is taken as a 0.02 per cent proof stress, equation (7) gives a value of 228 MPa, compared to the monotonic yield of 392 MPa which was used in Fig. 1. The 0.02 per cent proof stress, if substituted in equation (3), implies that the allowable stress range for LEFM calculation is only 152 MPa, at which there is just 0.16 per cent deviation from the LEFM line of slope minus one half on Fig. 6. Thus, for this material, equation (3) provides a very stiff restriction on the use of LEFM. However, in general, for a material following the Ramberg–Osgood formulation, the percentage deviation of the stress range from the elastic line at 2/3 of the 0.02 per cent proof stress is given by x, where

$$x = (E/k)(3)^{1-1/n}(0.0002)^{1-n} \times 100 \text{ per cent} \quad (8)$$

and E, k, and n are the elastic modulus, cyclic strength coefficient, and cyclic strain hardening exponent, respectively. This formula is particularly sensitive to the value of n; for example a strain hardening exponent of 0.3 gives a

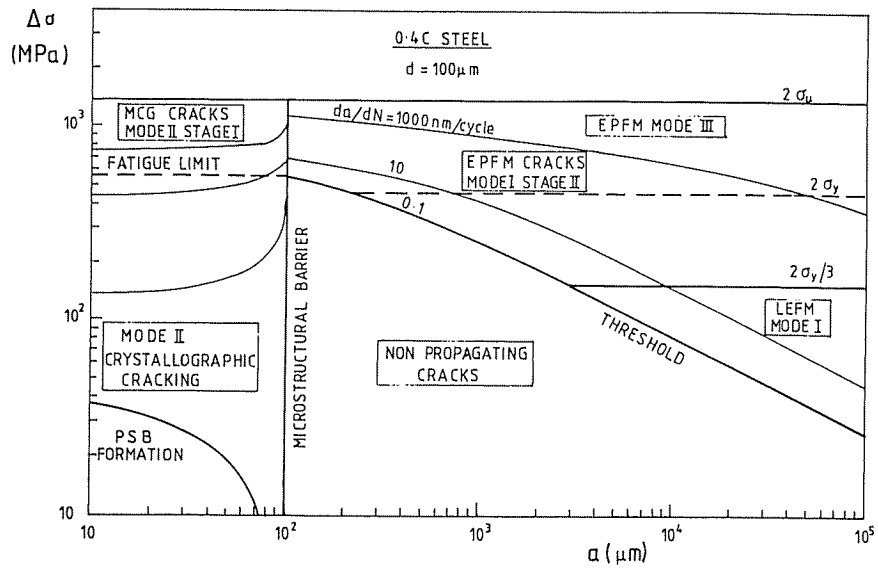

Fig 7 Fatigue diagram for 0.4C steel, based on equations (4) and (5)

deviation of 3.5 per cent, justifying the choice of the LEFM boundary at $2\sigma_y/3$ as reasonable.

Interfaces between crack growth regimes

The fatigue diagram of Fig. 6 has been replotted in Fig. 7 with six distinct regimes of crack behaviour defined. As in the Kitagawa–Takahashi diagram, the LEFM regime is limited by the horizontal line at $2\sigma_y/3$, with lower bound crack lengths given by the fatigue threshold condition. Below-threshold non-propagating cracks exist, but the microstructural barrier, characterized by the dimension d, gives a lower bound crack length to this regime.

The upper bound to EPFM behaviour must correspond with the tensile strength σ_u = 683 MPa, i.e., for fully reversed cycling, $2\sigma_u$. This line indicates the special case of infinite crack growth rate. However, the EPFM regime can be subdivided into two regimes corresponding to Mode I behaviour and, at higher stresses, Mode III cracking. It has not yet been shown conclusively what constitutes the critical condition for a transition to Mode III, but such transitions have been observed regularly (**22**), and the preference for Mode I at low stress and Mode III at high stress has been elegantly demonstrated by Ritchie *et al.* (**23**). It is possible that the transition to Mode III relates principally to yield stress, i.e., the line $2\sigma_y$ in Fig. 7, but it is more likely that a higher stress range is required for the tearing mechanism to dominate.

Considering microstructurally short cracks, above the fatigue limit these correspond to Stage I crack growth, as discussed previously. However, the fatigue limit stress is not necessarily a limit on the MCG mechanism, and Mode II cracks are free to develop on crystallographic slip systems well below the fatigue limit stress. Although equation (4) provides no lower limit of strain or stress for MCG, it is reasonable to assume that microscopic plasticity is an essential feature of crack extension, if only to provide the necessary irreversibility of deformation. Since many such cracks propagate along persistent slip bands (PSB), a very tentative lower bound to the crystallographic cracking region has been drawn in Fig. 7 by using a resolved shear stress range for PSB formation of 98 MPa, observed in α iron (**14**). In addition a stress concentration factor of 5 for the defect of length a acting on a net section stress, taken over the ligament between a and d, was assumed to determine the resolved shear stress on the PSB that must emanate from the crack tip. In spite of the lack of rigour in these three assumptions, it is nevertheless apparent that the lower bound to the Mode II cracking regime is an order of magnitude below the fatigue limit. Non-propagating fatigue cracks have been observed both in short crack studies (**24**) below the fatigue limit and in mixed mode LEFM experiments well below the Mode I threshold (**25**), and in both cases the cracks arrested on reaching defined microstructural features.

The fatigue diagram in Fig. 7 shows the six regimes of crack growth behaviour, together with lines denoting the interfaces between each regime, labelled with the principal physical causes for each interface. It is also apparent that the three fundamental modes of cracking, traditionally defined in fracture mechanics texts, each have a distinctive role to play in the process of fatigue failure. Although specific laws, equations (4) and (5) for 0.4C steel, have been used to derive Fig. 7, it appears that the general form of this diagram can have a much wider applicability to most, and probably all, ductile metals. The

Table 1 Regimes of crack propagation

Type	*Mode*	*Stage*	*Equation*	*Mechanism*	*Crack length limits*	*Stress limits*
LEFM	I	—	5	Striation	$a > a_{th}$	$\Delta\sigma < 2\sigma_y/3$
EPFM	I	II	5	Striation	$a > a_{th}$ $a > a_M$	$\Delta\sigma < A\sigma_y$
EPFM	III	III	*	Tearing	$a > a_{th}$ $a > a_M$	$A\sigma_y < \Delta\sigma < 2\sigma_u$
MCG	II	I	4	Crystallographic shear	$a < a_M$	$\Delta\sigma_{fl} < \Delta\sigma < 2\sigma_u$
CC†	II	—	4	Crystallographic shear (PSB)	$a < d$	$\Delta\sigma_{PSB} < \Delta\sigma < \Delta\sigma_{fl}$
NPC‡	I/II	—	1	$a < a_{th}$	$d < a < a_{th}$	$\Delta\sigma < \Delta\sigma_{fl}$

* See (**22**).
† CC: crystallographic cracking.
‡ NPC: non-propagating cracks

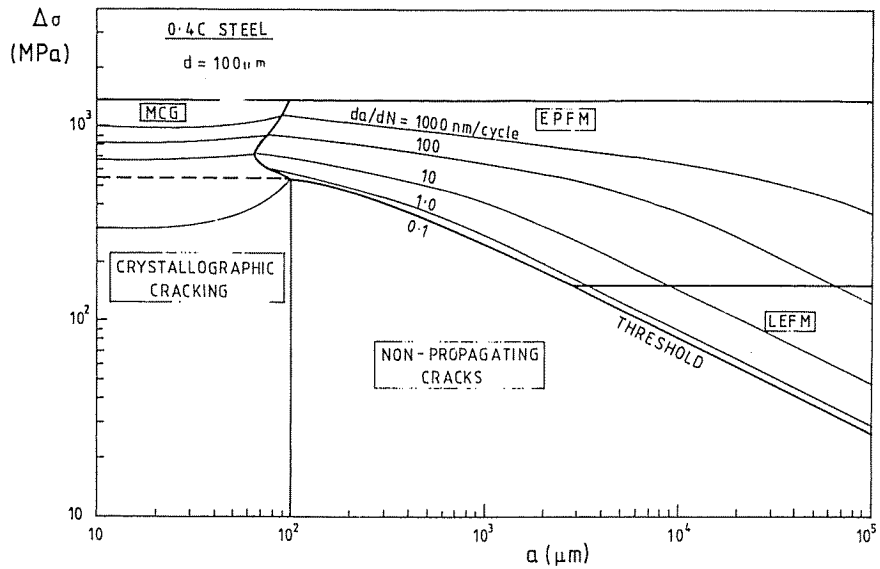

Fig 8 Fatigue diagram for 0.4C steel with reduced microstructural crack growth rates (equation (9))

interface lines separating each regime may move considerably with a change of properties, such as yield stress, fracture ductility, microstructure, etc., but these six regimes will remain, with the possible addition of other mechanisms for propagation. The basic types of propagation are listed in Table 1.

As an example, Fig. 8 has been drawn using equation (5) for EPFM cracks, but with a different MCG equation

$$da/dN = 1069(\Delta\varepsilon)^{3.18}(d - a) \qquad (9)$$

derived for the same material (**26**). Whereas the right-hand side of the figure is unchanged, the MCG regime is reduced in extent, illustrating a significant feature of Pineau's criterion in that the transition to Mode I can occur before the microstructural barrier is reached. This is because the MCG rates from equation (9) are considerably lower than those of equation (4). Although the transition to fracture mechanics control generally occurs at grain boundaries, or other microstructural features (**18**), this is not always the case, as in, for example, single crystals (**27**).

Discussion

The fatigue diagram, plotted from crack growth rate considerations, provides a logical basis for the frequently observed shape of the Kitagawa–Takahashi diagram. While Fig. 7 has been developed for the specific case of 0.4C steel,

with just one microstructural morphology, expressions of the type given by equations (4) and (5) in this paper only provide a convenient vehicle with which to derive the fatigue diagram. It's basic form, showing six different regions of crack growth, is of general applicability, since it is sufficient for the actual crack propagation laws to have (1) a region of MCG where growth rate decreases as crack length increases, (2) a region of fracture mechanics controlled fatigue where growth rate increases with crack length, and (3) a well defined fatigue threshold for long cracks.

The diagram in Fig. 7 has been based on stress range in order to relate to the well known Kitagawa–Takahashi diagram. This may be the most convenient form while designers continue to use *S–N* data in infinite life fatigue assessments. However, a strain based diagram, e.g., Fig. 4, presents a simpler picture, relates to strain controlled fatigue design methods used for finite life assessments, and, insofar as the simple EPFM equation (5) remains applicable as originally proposed by Boettner *et al.* (**28**)–(**30**)(**2**), it obviates the need to distinguish the region of validity for LEFM. Furthermore, for Mode III crack growth it has been shown that the use of a strain intensity parameter enables crack growth rates to be represented by simple equations which should facilitate the inclusion of a Mode I/Mode III transition on the diagram (**22**)(**23**).

The effects of both mean stress and multiaxial loading should be assessed from the point of view of design utility. This may prove difficult while maintaining a two dimensional plot, but the concepts embodied in the Goodman diagram show how at least the low stress fatigue behaviour might be represented in three dimensions, the third axis relating to mean stress. Work on multiaxial effects for both short cracks (**26**), LEFM cracks (**31**), and EPFM cracks (**32**)(**33**) indicates how equations (4) and (5) can be extended to describe Mode II and Mode I behaviour, respectively, but considerable work is required on Mode III (**34**) before a multiaxial stress fatigue diagram can be completed.

The interface lines have been discussed above, but it is clear that so far as MCG is concerned, the choice of d, the characteristic microstructural dimension for an individual crack, is crucial. Many papers in this volume show that a variety of microstructural barriers can arise, and for any metal or alloy, it is important from a design viewpoint not to underestimate the value of d. If the crack growth obstacles are not strong, and cracks penetrate and keep on propagating from one obstacle to the next, albeit very slowly, then no definite fatigue limit will be obtained. This is the case for many aluminium alloys, for example (**35**). Obstacles may take a variety of forms, such as grain boundaries, triple points, second phases of high strength, pearlite, large inclusions, or precipitates. A good example of grain boundaries acting as highly effective barriers to slip is given by Kompek *et al.* (**36**) for low carbon steels, and correspondingly, they may arrest microstructural fatigue cracks. In the particular case of 0.4C steel studied by Hobson, the dominant barrier was pearlite, being of high strength compared to the ferrite in which cracks nucleated. Thus d could also be estimated from a statistical analysis of the microstructure to find the greatest linear ferrite path between pearlite colonies. The concept of pearlite as a crack growth barrier is not new, and for textured steels the relationship between crack growth direction (or mode) and the local texture has an important bearing on the fatigue strength (**37**), for both short and long cracks.

The limitations to LEFM applicability have received much attention in the literature (**8**)(**2**)(**7**), and equation (3) may appear to be unduly restrictive for some materials. However, simple rules for predicting l_2, the crack length above which LEFM can be used (**8**), are liable to give non-conservative estimates for metals with low yield stress and high strain hardening exponents, if the prediction of equation (8) is correct.

The development of MCG is frequently cited in the literature as being associated with the PSB. However, this is not always the case, and Mode II cracks have been observed to form on grain boundaries due to incompatibility of deformation in adjacent grains (**38**). Other mechanisms for crack nucleation could be postulated, such as corrosive attack; therefore, the lower bound to the crystallographic cracking regime should be estimated according to the relevant mechanism for the material and environment concerned.

The fatigue diagram provides a visual method of selecting the correct mechanism, together with the corresponding characteristic equation and crack growth mode, for any crack size and stress level. This is an important choice for the scientist assessing fatigue crack behaviour, and also for the designer seeking to use a defect tolerant approach to finite life prediction or remnant life assessment.

Conclusions

Various distinct regimes of short and long crack growth in fatigue have been identified, each with separate mechanisms for crack extension. Since it is inappropriate to use a model for one mechanism when examining data related to another mode of cracking, a fatigue diagram has been proposed to show which is the dominant mode of growth for any given stress range and crack length.

Such diagrams may be used to interpret the Kitagawa–Takahashi diagram, to predict the history of a crack under general loading, and to estimate the fatigue limit for a known microstructural morphology.

Acknowledgements

The author is indebted to the Central Electricity Generating Board for a Research Fellowship. The concepts developed in this paper are the direct result of detailed investigations by numerous research students and visitors in the fracture research group at the Mechanical Engineering Department, Sheffield University.

References

(1) LANKFORD, J. (1985) The influence of microstructure on the growth of small fatigue cracks, *Fatigue Fracture Engng Mater. Structures*, **8**, 161–175.

(2) SKELTON, R. P. (1982) Growth of short cracks during high strain fatigue and thermal cycling, *ASTM STP 770* (American Society for Testing and Materials, Philadelphia), pp. 337–381.

(3) TAYLOR, D. and KNOTT, J. F. (1981) Fatigue crack propagation behaviour of short cracks; the effect of microstructure, *Fatigue Engng Mater. Structures*, **4**, 147–155.

(4) MUGHRABI, H. (1980) Microscopic mechanisms of metal fatigue, *Strength of metals and alloys* (Edited by P. Haasen, V. Gerold, and G. Kostorz), Vol. III (Pergamon, Oxford), pp. 1615–1638.

(5) KITAGAWA, H. and TAKAHASHI, S. (1976) Applicability of fracture mechanics to very small cracks or the cracks in the early stage, *Proc. 2nd Int. Conf. Mech. Behaviour of Materials*, Boston, pp. 627–631.

(6) KNOTT, J. F. (1973) *Fundamentals of fracture mechanics* (Butterworths, London), p. 134.

(7) MILLER, K. J. (1984) Initiation and growth rates of short fatigue cracks, *Fundamentals of deformation and fracture* (Edited by B. A. Bilby, K. J. Miller, and J. R. Willis) (Cambridge University Press), pp. 477–500.

(8) TAYLOR, D. (1984) The effect of crack length on fatigue threshold, *Fatigue Engng Mater. Structures*, **7**, 267–277.

(9) DE LOS RIOS, E. R., TANG, Z., and MILLER, K. J. (1984) Short crack fatigue behaviour in a medium carbon steel, *Fatigue Engng Mater. Structures*, **7**, 97–108.

(10) NAM SOON CHANG and HAWORTH, W. L. (1985) Fatigue crack initiation and early growth in an austenitic stainless steel, *Proc. 7th Int. Conf. Strength of Metals and Alloys*, Vol. II (Pergamon Press, Oxford), pp. 1225–1230.

(11) HOBSON, P. D. (1985) The growth of short fatigue cracks in a medium carbon steel, PhD thesis, University of Sheffield.

(12) HOBSON, P. D., BROWN, M. W., and DE LOS RIOS, E. R. (1986) Two phases of short crack growth in a carbon steel, *The behaviour of short fatigue cracks* (Edited by K. J. Miller and E. R. de los Rios), (Mechanical Engineering Publications, London), pp. 441–459 (This volume).

(13) LANKFORD, J. (1982) The growth of small fatigue cracks in 7075-T6 aluminium, *Fatigue Engng Mater. Structures*, **5**, 233–248.

(14) HOURLIER, F., d'HONDT, H., TRUCHON, M., and PINEAU, A. (1985) Fatigue crack path behaviour under polymodal fatigue, *ASTM STP 853* (American Society for Testing and Materials, Philadelphia), pp. 228–248.

(15) BROWN, M. W. and MILLER, K. J. (1979) Initiation and growth of cracks in biaxial fatigue, *Fatigue Engng Mater. Structures*, **1**, 231–246.

(16) DE LOS RIOS, E. R., MOHAMED, H. J., and MILLER, K. J. (1985) A micromechanics analysis for short fatigue crack growth, *Ibid*, **8**, 49–63.

(17) MILLER, K. J. and BROWN, M. W. (1984) Multiaxial fatigue: an introductory review, *Subcritical crack growth due to fatigue, stress corrosion and creep* (Edited by L. H. Larsson) (Elsevier Applied Science, London), pp. 215–238.

(18) PLUMBRIDGE, W. J. (1972) Review: fatigue-crack propagation in metallic and polymeric materials, *J. Mater. Sci.*, **7**, 939–962.

(19) HOBSON, P. D. (1982) The formulation of a crack growth equation for short cracks, *Fatigue Engng Mater. Structures*, **5**, 323–327.

(20) MARSH, D. J. (1981) A thermal shock fatigue study of type 304 and 316 stainless steels, *Fatigue Engng Mater. Structures*, **4**, 179–195.

(21) IBRAHIM, M. F. E. (1981) *Early damage accumulation in metal fatigue*, PhD thesis, University of Sheffield.

(22) HAY, E. and BROWN, M. W. (1986) Initiation and early growth of fatigue cracks from a circumferential notch loaded in torsion, *The behaviour of short fatigue cracks* (Edited by K. J. Miller and E. R. de los Rios), (Mechanical Engineering Publications, London), pp. 309–321 (This volume).

(23) RITCHIE, R. O., McCLINTOCK, F. A., NAYEB-HASHEMI, H., and RITTER, M. A. (1982) Mode III fatigue crack propagation in low alloy steel, *Met. Trans*, **13A**, 101–110.

(24) MILLER, K. J., MOHAMED, H. J. and DE LOS RIOS, E. R. (1986) Fatigue damage accumulation above and below the fatigue limit, *The behaviour of short fatigue cracks* (Edited by K. J. Miller and E. R. de los Rios), (Mechanical Engineering Publications, London), pp. 491–511 (This volume).

(25) GAO, H., BROWN, M. W., and MILLER, K. J. (1982) Mixed-mode fatigue thresholds, *Fatigue Engng Mater. Structures*, **5**, 1–17.

(26) PEREZ CARBONELL, E. and BROWN, M. W. (1986) A study of short crack growth in torsional low cycle fatigue for a medium carbon steel, *Fatigue Engng Mater. Structures*, **9**, 15–33.

(27) KLESNIL, M. and LUKAS, P. (1969) Dislocation substructure associated with propagating fatigue crack, *2nd Int. Conf. Fracture*, Brighton, pp. 725–730.

(28) BOETTNER, R. C., LAIRD, C., and McEVILY, A. J. (1965) Crack nucleation and growth in high strain low cycle fatigue, *Trans Met. Soc. AIME*, **233**, 379–387.

(29) HAIGH, J. R. and SKELTON, R. P. (1978) A strain intensity approach to high temperature fatigue crack growth and failure, *Mater. Sci. Engng*, **36**, 133–137.

(30) TOMKINS, B. (1975) The development of fatigue crack propagation models for engineering applications at elevated temperatures, *J. Engng Mater. Tech.*, **97H**, 289–297.

(31) KITAGAWA, H., YUUKI, R., TOHGO, K., and TANABE, M. (1985) ΔK-dependency of fatigue growth of single and mixed mode cracks under biaxial stress, *ASTM STP 853* (American Society for Testing and Materials, Philadelphia), pp. 164–183.

(32) BROWN, M. W. and MILLER, K. J. (1985) Mode I fatigue crack growth under biaxial stress at room and elevated temperature, *ASTM STP 853*, pp. 135–152.

(33) BROWN, M. W., DE LOS RIOS, E. R., and MILLER, K. J. (1984) A critical comparison of proposed parameters for high strain fatigue crack growth, *ASTM Symp. on Fundamental Questions and Critical Experiments in Fatigue*, Dallas.

(34) MILLER, K. J. and BROWN, M. W. (Editors) (1985) *Multiaxial fatigue*, *ASTM STP 853* (American Society for Testing and Materials, Philadelphia), pp. 203–377.

(35) BLOM, A. F., FATHULLA, A., HEDLUND, A., STICKLER, R., and WEISS, B. (1986) Short fatigue crack growth behaviour in Al-2024 and Al-7475 alloys, *The behaviour of short fatigue cracks* (Edited by K. J. Miller and E. R. de los Rios), (Mechanical Engineering Publications, London), pp. 37–66 (This volume).

(36) KOMPEK, G., MATZER, F. E., and MAURER, K. L. (1982) Crack initiation and crack propagation by torsional fatigue in low carbon steels, *Fracture and the role of microstructure* (Edited by K. L. Mauer and F. E. Matzer), (EMAS, Warley), Vol. 2, pp. 398–406.

(37) OHJI, K., OGURA, K., and HARADA, S. (1975) Observation of low cycle fatigue crack initiation and propagation in anisotropic rolled steel under biaxial stressing, *Bull. Japan Soc. Mech. Engrs*, **18**, 17–24.

(38) GUIU, F., DULNIAK, R., and EDWARDS, B. C. (1982) On the nucleation of fatigue cracks in pure polycrystalline α-iron, *Fatigue Engng Mater. Structures*, **5**, 311–321.